Published Online on 29 June 2016

Proc Indian Natn Sci Acad **82** No. 2 June Spl Issue 2016 pp. 147-162

DOI: 10.16943/ptinsa/2016/48409

Research Paper

Parallel Partitioned Simulations of Real World's Coupled Problems

S YOSHIMURA*,[1] and T YAMADA[2]
[1]*Department of Systems Innovation, School of Engineering, The University of Tokyo, Japan*
[2]*RACE, The University of Tokyo, Japan*

(Received on 24 April 2016; Accepted on 28 April 2016)

We have been developing a parallel partitioned simulation system to solve large scale real world's coupled problems. This paper describes some key technologies of the system, and demonstrates its practical performance and effectiveness through solving various kinds of real world's problems.

Keywords: Coupled Analysis; Partitioned Approach; Parallel Computing; FSI.

Introduction

Fluid-structure interaction (FSI) is an interdependent phenomenon between fluid and structure that affects their dynamic behaviors. Since there are a variety of FSI problems in engineering, science, medicine and daily life, it is very important to understand and to solve FSI problems. Even though focusing only on structural problems, there are a variety of coupled phenomena such as:

(a) FSI,

(b) Thermal–FSI,

(c) Electromagnetic–Structure Interaction,

(d) Electromagnetic–FSI,

(e) Acoustic–Structure Interaction,

(f) Soil–Structure Interaction,

(g) Control–Structure Interaction,

(h) Electromagnetic–Acoustic–Control–Structure Interaction, and others.

Many researchers have attempted to develop numerical methods for solving FSI problems with improved accuracy, problem scale, stability, robustness, and efficiency (for example, Mittal S and Tezduyar T E, 1992; Farhat C and Lessoine M, 2000; Ohayon R, 2001; Basilevs *et al.*, 2013). Those previous studies have made significant progress, but there are still strong demands for further researches on shortening computation time,increasing the degrees of freedom (DOFs) of models and dealing with a variety of phenomena in a generalized manner in order to solve real world's coupled problems of complex machines and structures. Thus we have been developing an efficient and robust simulation system to solve a variety of large-scale coupled problems in parallel computing environments (Kataoka *et al.*, 2014; Yoshimura *et al.*, 2015a; Yamada *et al.*, Accepted).

In general, coupled phenomena can be solved by either monolithic or partitioned approaches. In the monolithic approaches (for example, Zhang and Hisada, 2001; Mandel, 2002; Heil, 2004; Ishihara and Yoshimura, 2005; Tezduyar *et al.*, 2006; Dettmer and Peric, 2006; Minami *et al.*, 2011), the governing equations describing fluid and structure parts with their interface conditions are formed into a single system of equations, allowing the equations to be solved simultaneously. On the other hand, those governing equations are solved separately in the partitioned approaches (for example, Fellippa and Park 1980; Le Tallec and Mouro, 2001; Park *et al.*, 2001; Michler *et al.*, 2004; Matthies *et al.*, 2006; Forster *et al.*, 2007; Jiang *et al.*, 2007).

**Author for Correspondence: E-mail: yoshi@sys.t.u-tokyo.ac.jp*

In our research, we focus on the partitioned approaches, because we can use appropriate techniques for solving fluid and structural equations, respectively. Furthermore, iterative partitioned approaches (for example, Küttler and Wall, 2008, 2009; Yamada and Yoshimura, 2008; Degroote *et al.*, 2009; Minami and Yoshimura, 2010) have recently attracted a great deal of attention because they can improve accuracy and robustness in comparison with simple partitioned ones. In the approaches, fluid and structural equations are solved separately and iteratively at each time step until the interface conditions of equilibrium and continuity are satisfied.

This paper describes some key technologies of oursystem, and demonstrates its practical performance and effectiveness through solving various kinds of real world's coupled problems.

Governing Equations

Figure 1 illustrates a typical FSI problems. The problem consists of two domains, a fluid domain W^F and a structure domain W^S. The two domains share an FSI interface Γ_{FSI}.

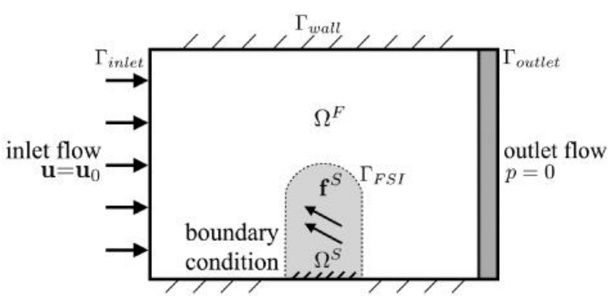

Fig. 1: Basic FSI problem

Fluid Domain

The fluid domain is governed by the following Navier-Stokes equation in an arbitrary Lagrangian-Eulerian (ALE) frame of reference :

$$\rho^F\left(\frac{\partial \boldsymbol{u}}{\partial t}+(\boldsymbol{u}-\hat{\boldsymbol{u}})\cdot\nabla\boldsymbol{u}\right)-\nabla\cdot\sigma^F=\boldsymbol{f}^F \tag{1}$$

and the continuity equation :

$$\nabla\cdot\boldsymbol{u}=0, \tag{2}$$

where ρ^F is the density of the fluid, $\boldsymbol{u}$ is the velocity vector of the fluid, $\hat{\boldsymbol{u}}$ is the mesh velocity vector, $\boldsymbol{\sigma}^F$ is the stress tensor of the fluid, and $\boldsymbol{f}^F$ is the external force vector applied to the fluid. Eq. (1) is derived by substituting the following stress tensor $\boldsymbol{\sigma}^F$ of the fluid into the Cauchy momentum equation :

$$\sigma^{\boldsymbol{F}}=-p\boldsymbol{I}+2\mu\boldsymbol{D}, \tag{3}$$

where p is the pressure of the fluid, $\boldsymbol{I}$ is the unit tensor, μ is the viscosity of the fluid, and $\boldsymbol{D}$ is the deformation rate tensor.

Structure Domain

The structure domain is governed by the Cauchy momentum equation of the Saint Venant-Kirchhof model considering geometric nonlinearity :

$$\rho^S\frac{\partial^2\boldsymbol{d}}{\partial t^2}-\nabla\cdot\sigma^S=\boldsymbol{f}^S \tag{4}$$

where ρ^S is the density of the structure, $\boldsymbol{d}$ is the displacement vector of the structure, $\boldsymbol{\sigma}^S$ is the stress tensor of the structure, and $\boldsymbol{f}^S$ is the external force vector applied to the structure. $\boldsymbol{\sigma}^S$ is given by

$$\sigma^S=E\cdot\varepsilon^S, \tag{5}$$

where $\boldsymbol{E}$ is the elasticity tensor of the structure and ε^S is the strain tensor of the structure.

Interface between Fluid and Structure Domains

At the FSI interface Γ_{FSI}, the following conditions of continuity and stress equilibrium must be fulfilled,

$$\int \boldsymbol{u}dt=\boldsymbol{d} \text{ on } \Gamma_{FSI} \tag{6}$$

$$\sigma^F\cdot\boldsymbol{n}^F+\sigma^S\cdot\boldsymbol{n}^S=0 \text{ on } \Gamma_{FSI} \tag{7}$$

where $\boldsymbol{n}^F$ and $\boldsymbol{n}^S$ are the unit normal vectors of the fluid and the structure, respectively, at the interface.

Iterative Partitioned Coupling Methods

The iterative partitioned coupling method divides an original FSI problem into the following three components : fluid analysis *F*, structure analysis *S*, and mesh control *M*. In the problem, the governing equations of the fluid, structure, and mesh control must satisfy the conditions of continuity and equilibrium at the FSI interface.

Redefinition of FSI Problem

Each component is treated as a nonlinear problem in the following :

$$\boldsymbol{X}_\Gamma^{k+1} = M(\boldsymbol{d}_\Gamma^k) \tag{8}$$

$$\left(\boldsymbol{u}_\Gamma^{k+1}, \boldsymbol{p}_\Gamma^{k+1}\right) = F(\boldsymbol{X}_\Gamma^{k+1}) \tag{9}$$

$$\boldsymbol{d}_\Gamma^{k+1} = S\left(\boldsymbol{u}_\Gamma^{k+1}, \boldsymbol{p}_\Gamma^{k+1}\right), \tag{10}$$

where $\boldsymbol{X}$ is the mesh coordinate and $\boldsymbol{p}$ is the pressure of the fluid. The superscript k and subscript Γ represent the k-th iteration and the variables at the interface, respectively. At each time step, Eqs. (8)-(10) are solved sequentially and iteratively until the final solution, which satisfies the following nonlinear equation, is obtained :

$$\boldsymbol{d}_\Gamma = S\left(F(M(\boldsymbol{d}_\Gamma))\right) \tag{11}$$

The residual $\mathbf{r}$ of the above nonlinear equation is defined as :

$$r(\boldsymbol{d}_\Gamma) \equiv \boldsymbol{d}_\Gamma - S(F(M(\boldsymbol{d}_\Gamma))). \tag{12}$$

Thus, an iterative partitioned method can be considered as the process of seeking the displacement $\boldsymbol{d}_\Gamma$ of the structure at the FSI interface that minimizes the above residual.

Parallel Coupling Technologies

Our coupled simulation approach consists of the following three basic philosophies :

(1) Partitioned approach to use various kinds of existing solvers optimized for parallel computers such as a parallel structure solver, ADVENTURE (Yoshimura *et al.*, 2002; Ogino *et al.*, 2005; Yoshimura *et al.*, 2015a; Yoshimura *et al.*, 2015b) and a parallel flow solver, FrontFlow/blue (FFB) (Kato *et al.*, 2003, 2005),

(2) Fixed point iteration to improve accuracy and robustness although added mass effects are still big issues for partitioned approaches, and

(3) Parallel coupling tool named ADVENTURE_Coupler (Kataoka *et al.*, 2014; Yamada *et al.*, Accepted) and its family to integrate two or more independent parallel solvers with only minimum modification to them.

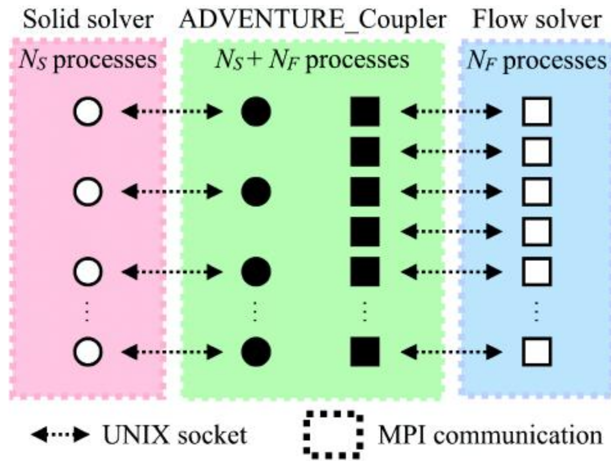

Fig. 2: Communication model of coupled analysis using ADVENTURE_Coupler

Among various iterative coupled algorithms in literature, we have selected some algorithms meeting the following three criteria :

(a) Robust convergence,

(b) Ability to treat each parallel solver as black box, and

(c) Easy and efficient parallelization.

Finally, Gauss Seidel, matrix free Newton-Krylov and Quasi-Newton methods such as Broyden method (Charles and Broyden, 1965) have been selected (Minami and Yoshimura, 2010), and implemented into the Coupler (Kataoka *et al.*, 2014; Yamada *et al.*, Accepted).

Figure 2 shows the parallel communication model using the Coupler. Flow and structure analysis solvers are assumed to be parallelized using MPI libraries. The coupler handles interface variables using subprocesses corresponding to the processes of the flow and structure solvers. The Coupler runs with $N_F + N_S$ parallel subprocesses, where the numbers of processes run by the flow and structure solvers are N_F and N_S, respectively. The UNIX socket is used to communicate between each analysis solver and the Coupler. The data transmission and the interpolation of interface variables from one mesh to another are executed within the processes of the Coupler. The Coupler realizes automatic construction of mapping relation between complex-shaped interface surfaces considering different mesh subdivision and different subdomain decomposition as schematically illustrated in Fig. 3. The interface variables are interpolated using the shape functions of the elements.

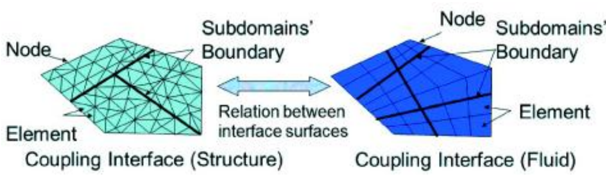

Fig. 3: Schematic view of automatic construction of mapping relation between complex-shaped interface surfaces

To perform coupled analysis, only a few communication libraries, which are called ADVENTURE_Coupler libraries, are required for integration into parallel solvers. In each solver, some IO portions are just replaced with the communication libraries. Thanks to them, a whole coupled simulation process can be fully parallelized.

The overall analysis flow is shown in Fig. 4. In the iterative partitioned analysis, fixed-point iteration is executed. At each time step of the analysis, the displacement of the structure is calculated by the structure solver, and that at the FSI interface is transmitted through the Coupler to the flow solver. The flow solver controls the fluid mesh and calculates the velocity and pressure of the fluid. The velocity and pressure at the FSI interface are then transmitted back to the structure solver through the Coupler. The structure solver then again calculates the displacement

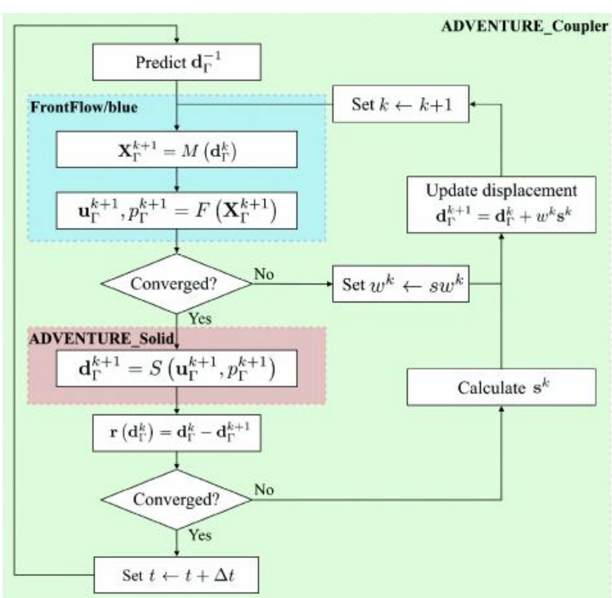

Fig. 4: Analysis flow

of the structure. After the fixed-point iteration converges, the analysis processes to the next time step, and the Coupler provides the initial value of the displacement of the structure. However, if the iteration does not converge, the analysis starts again within the current time step by changing the initial value using the line-search technique.

Applications

The developed simulation system has been applied to solve various coupled problems, i.e. (1) Seismic response of nuclear fuel assemblies set in fluid (Kataoka *et al.*, 2014), (2) Flow past square cylinder with thin plate (Yamada *et al.*, accepted), (3) Flapping flight of elastic wing (Yamada *et al.*, accepted), (4) Flow-induced vibration and noise of automobile (Yamade *et al.*, 2016; Iida *et al.*, 2016). Those are explained next.

Seismic Response of Nuclear Fuel Assemblies Set in Fluid

The purpose of this analysis is to investigate dynamic response behaviors of fuel assemblies in a Boiling Water Reactor (BWR) under seismic loading (Kataoka *et al.*, 2014; Yoshimura *et al.*, 2015c).

NUPEC's Demonstration Test

The experimental setup for dynamic responses of 368 fuel assemblies of Boiling Water Reactor (BWR) core are shown schematically in Fig. 5. This demonstration test was conducted in 1986 as one of the seismic proving tests of a BWR by the Nuclear Power Engineering Corporation (NUPEC) (NUPEC, 1988). The tested setup was a full-scale mock-up of the reactor core internals of the improved and standardized 1,100-MWe plant in a highly seismic zone. The setup consisted of the fuel assemblies, top guide, core plate, control rod guide tubes, control rod, control rod drive unit and core shroud. These were placed in an outer vessel filled with water. The vessel, placed on a shaking table, was vibrated horizontally. The time history of input wave is shown in Fig. 6. It is an artificial seismic wave with a frequency range of 3-12Hz. The frequency range includes the dominant frequency at the core plate on which the fuel assemblies are located. The demonstration test was conducted at room temperature and under atmospheric pressure.

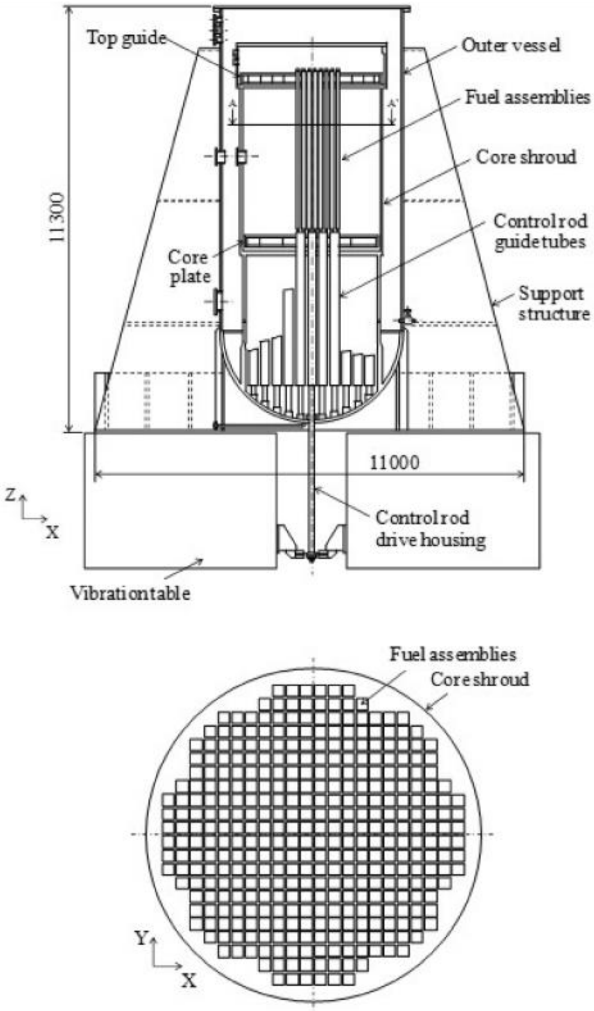

Fig. 5: Schematic of demonstration test

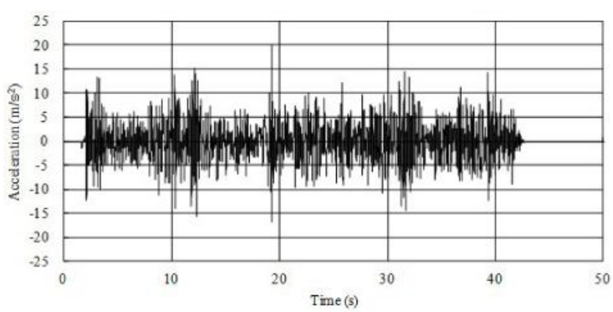

Fig. 6: Time history of input seismic wave

Numerical Model and Computer Used

A three dimensional finite element model shown in Fig. 7 is as follows. Both fluid and structure domains are discretized by tetrahedral elements. The total number of DOFs is approximately 10 million, i.e. the number of fluid nodes is 4,302,313 and that of the structure nodes is 2,048,960. The first resonant frequency of most fuel assemblies in the fluid is around 4.8Hz, and stiffness-proportional damping of Rayleigh's damping is employed, while setting the parameter so that the damping ratio becomes 7% at 4.8Hz. The time increment is set as $\Delta t = 0.005$ s because the sampling interval of the input seismic acceleration data is around 0.005 s. For this analysis, a PC cluster consisting of 8 personal computers is used. Each computer consists of one processor with 4 cores having 3.40 Hz and 16 GB memory. They are connected by Gigabit Ethernet. The average number of fixed-point iterations is 22.

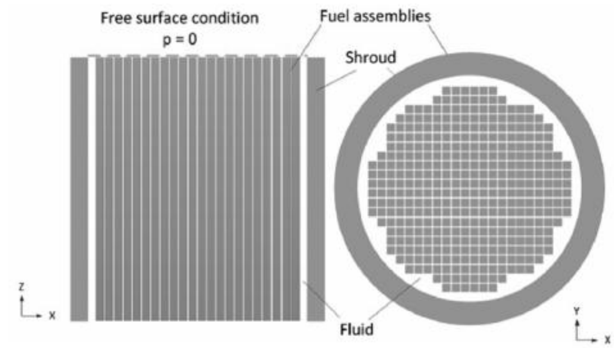

Fig. 7: Schematic of partitioned coupling model

Validation : Dynamic Responses

We discuss the comparison between numerical results and measured ones. Locations and IDs of the investigated fuel assemblies are illustrated in Fig. 8.

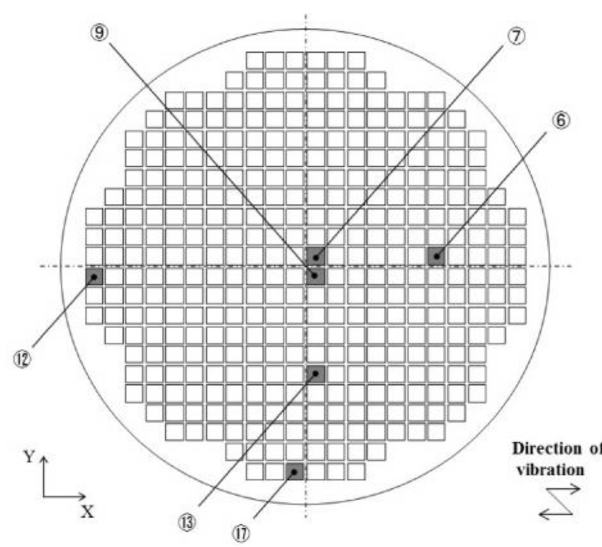

Fig. 8: Locations and IDs of evaluated fuel assemblies

The time histories of deflections at the axial center of the fuel assemblies are shown in Fig. 9. At first, it is again clearly shown from the figure that the dynamic response of the simulation results agrees well with the measured values at the demonstration test. As the result, the validity of the simulation method for such a realistic problem was confirmed.

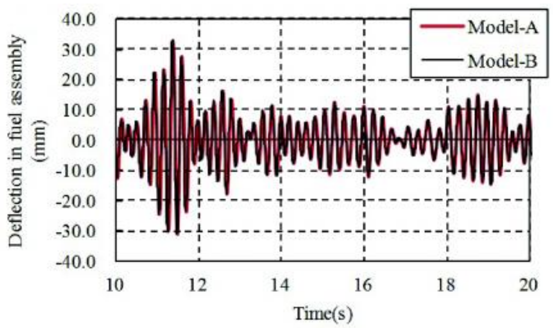

(A) Simulation results at Fuel 7

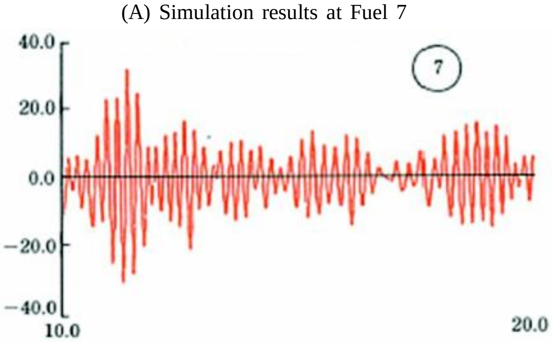

(B) Measured result of demonstration test at Fuel 7

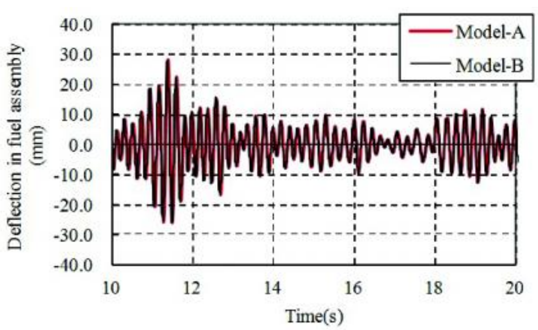

(A) Simulation results at Fuel 12

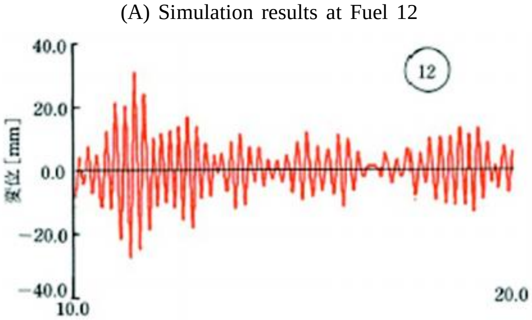

(B) Measured result of demonstration test at Fuel 12

Fig. 9: Time histories of deflection in representative fuel assemblies

Overall Behaviors of Fuel Assemblies

In the demonstration test, only a limited number of fuel assemblies were measured. In this study, thanks to superior characteristics of the numerical simulations, we have examined precise response behaviors of all 368 fuel assemblies. Figure 10 shows the histogram of calculated maximum deflection in the x-direction under seismic loading. It can be clearly observed that most fuel assemblies show almost identical seismic response. The standard deviation of the maximum seismic deflections was 4mm, which means that 68% of fuel assemblies in the core were within ± 4 mm of the average value. Thus, we have concluded that the vibration behavior of fuel assemblies was almost homogeneous.

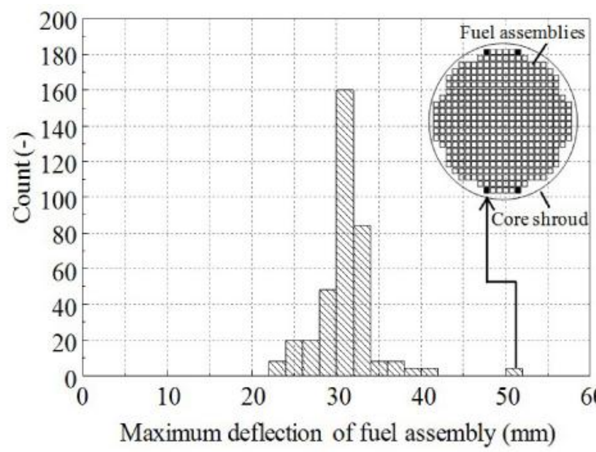

Fig. 10: Histogram of maximum seismic deflection

Figure 11 shows some results. The upper indicates that the variation in the maximum deflections of fuel assemblies is small and that a conventional single bar model often used for seismic design of BWR core is effective to some extent. The deflections of a few fuel assemblies located on the outer periphery were larger than those of the others. The nonuniformity of the relative locations of fuel assemblies on the outer periphery and the shroud is considered to be the reason for such behaviors.

Flow Past Square Cylinder with Thin Plate

To verify the developed FSI analysis system, we analyze a benchmark FSI problem: the vortex-induced oscillation of a flexible plate in the wake of a square column (Yamada *et al.*, accepted). The geometric

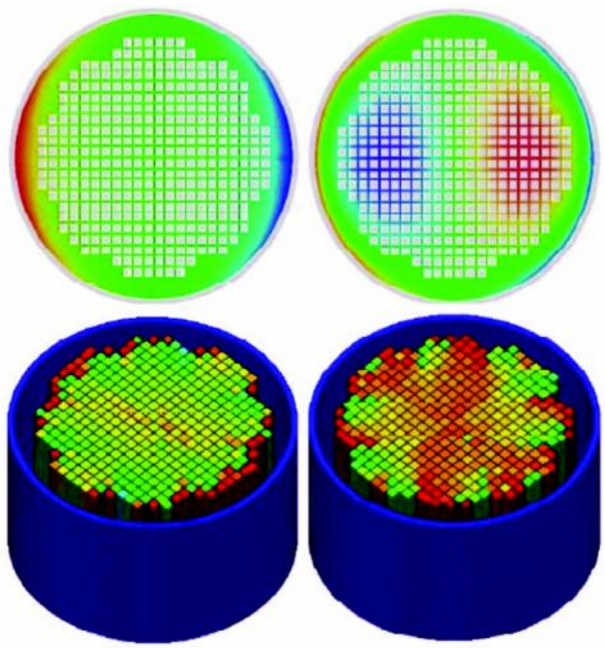

Fig. 11: Pressure distributions (Upper) and displacements of fuel rods (Lower) at the times t=2.7sec ad t=2.77sec

model of the problem is shown in Fig. 12. A square column is set in place, and a flexible plate is fixed at the downstream end of the column. As the inlet flow moves around the column and generates vortices,the structural oscillation of the plate occurs. This problem is usually simulated as a two-dimensional problem. Here this problem was solved using the developed three-dimensional FSI analysis system. The slip boundary condition is applied to all faces of the model except the inlet and outlet boundaries.The mesh partition of the fluid domain is shown in Fig. 13(A). The numbers of linear tetrahedral elements and nodes

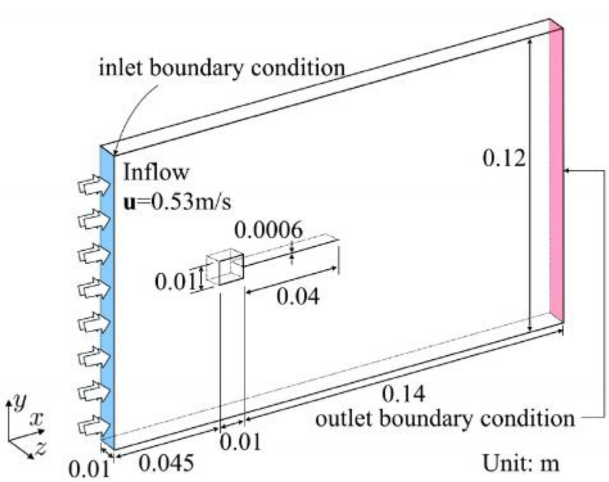

Fig. 12: Geometric model

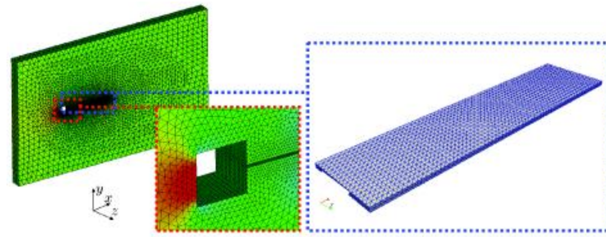

(A) **(B)**

Fig. 13: Meshes of fluid domain (A) and structure domain (B)

in the fluid domain are156,312 and 31,187, respectively. The mesh partition of the structure domain is shown in Fig. 13(B). We only partitioned the plate into structure meshes,considering the column as a wall in the fluid domain. In the structure domain,the numbers of quadratic tetrahedral elements and nodes are 14,234 and 24,367, respectively. The properties of the analysis model are as follows. The dynamic viscosity and density of the fluid are 0.35 Pa·s and 1.18 kg/m^3, respectively. The Young's modulus and density of the structure are 2.5 x 10^5 Pa and 100 kg/m^3, respectively. A PC cluster used for the analysis consisted of four PCs, each of which had 3.4 GHz quad-core Intel i7 2600 processor and16 GB of DDR3 memory.

In this analysis, we first conducted only fluid analysis to prepare the initial velocity and pressure fields. When a vortex began to form, we started the FSI analysis. The time step was set to 5.0 x 10^{-4} s. For the convergence criterion, $\varepsilon_{tol} = 10^{-3}$ was used in the fixed-point iteration, and an average of four iterations were required for each time step.

A snapshot of the pressure field showing the

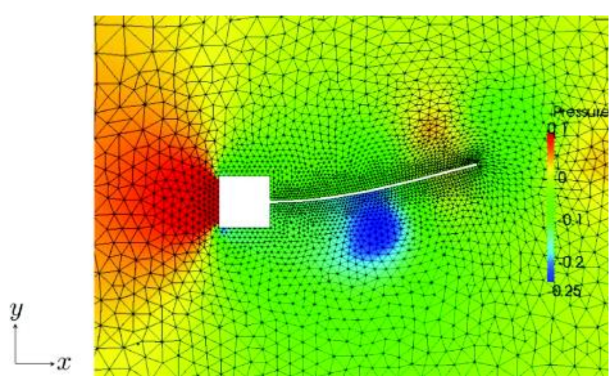

Fig. 14: Snapshot of pressure field showing the deformation of the model

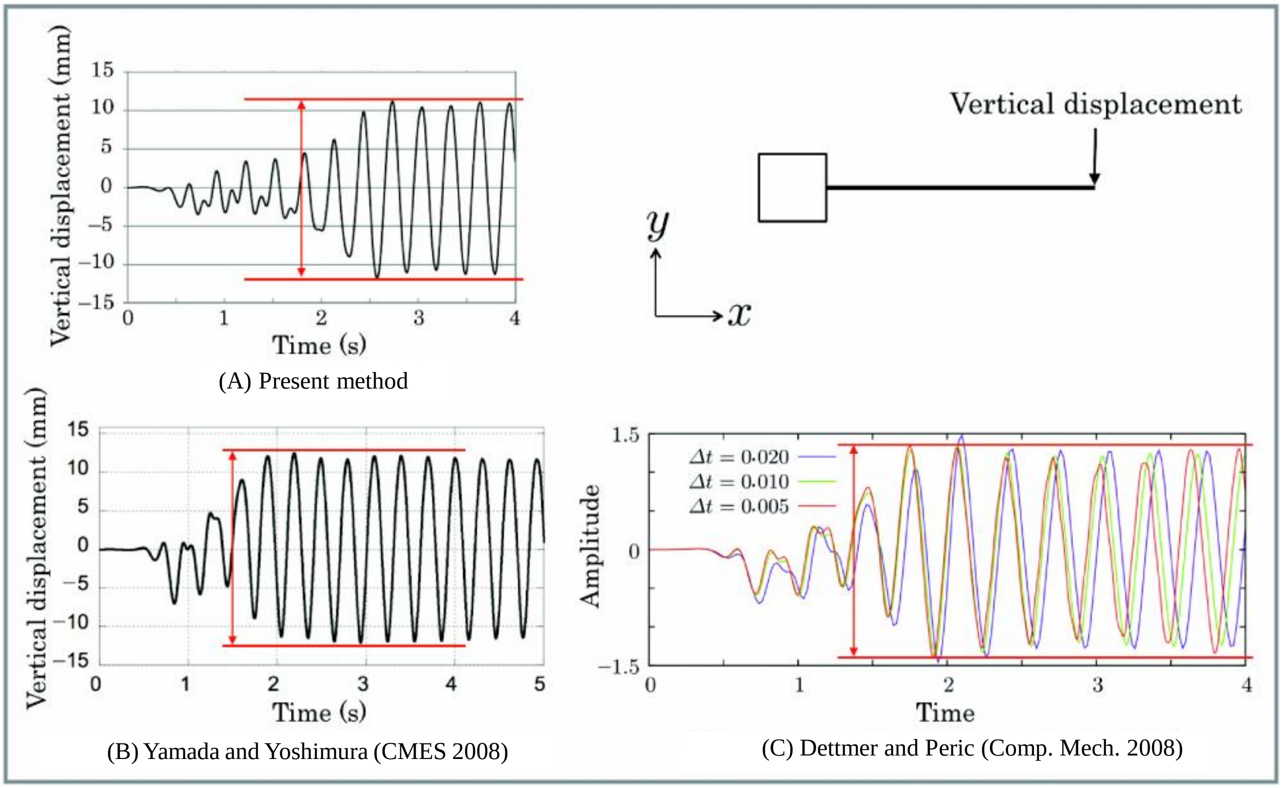

Fig. 15: Time history of the vertical displacement at the tip of the plate

deformation of the model is shown in Fig. 14. A time history of the vertical displacement at the tip of the plate is shown in Fig. 15(A). The plate started moving with increasing amplitude as the vortices approached it, but it entered a steady state when the amplitude reached 0.01 m. The frequency of the flapping of the plate in the steady state was approximately 3.2 Hz, which was close to the frequency of the structure itself (3.03 Hz), whereas the frequency of the vortex shedding was approximately 10 Hz when the Strouhal number was assumed to be 0.2. The amplitude obtained using the present method was almost the same as those obtained in the past studies (Yamada and Yoshimura, 2008; Dettmer and Peric, 2008), both of which were two-dimensional FSI simulations and obtained amplitudes slightly above 0.01 m. Thus, we concluded that thedeveloped FSI analysis system is able to solve the dynamic response to a flow excitation force with sufficient accuracy.

Flapping Flight of Elastic Wing

To demonstrate the practical application of the developed FSI analysis system, we analyzed the three-dimensional flapping motion of an elastic rectangular plate with the purpose of furthering the research and development of micro air vehicles (MAVs). The flapping of a wing, which is realized by birds and insects, is an unsteady aerodynamics problem. However, the aerodynamic performance of a flapping wing has not been yet perfectly evaluated by experimental studies. Full-scale three-dimensional simulations of flapping wings are still challenging to execute, although some studies have performed such simulations by the monolithic methods (Nakata and Liu, 2012; Takizawa *et al.*, 2014, 2015). We have also been working to solve this type of problem by

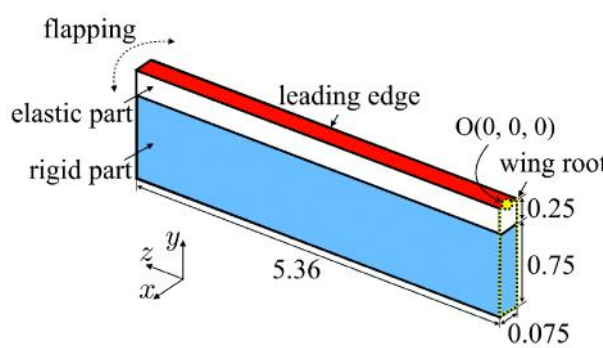

Fig. 16. Geometric model of the flapping wing

using the partitioned coupling approach (Yamada and Yoshimura, 2008; Yamada *et al.*, accepted). The aim of our series of simulation studies is not to computationally reproduce the flapping flight of actual birds or insects but to develop a design support tool for the optimization of the shape, structure, and motion of the flapping wings of MAVs. In this study, the developed FSI analysis system was applied to solve the flapping motion of an elastic rectangular plate.A geometric model of the structure is shown in Fig. 16. As the first step of our study, we focused on the flapping motion of one wing, omitting the body. The wing consists of two parts, i.e. an elastic part and a rigid part. The deformable flapping wing is located at the center of the fluid domain. To analyze the aerodynamic performance of hovering flight, we fix the end point node of the leading edge near the wing root. The flapping of the wing is initiated by applying a prescribed sinusoidal displacement to the leading edge. The prescribed motion of the leading edge of the wing is determined from two design variables: the maximum angle of flapping and the flapping frequency. The elastic part of the wing deforms, and the wing then passively enters the feathering mode. The slip boundary condition is applied to all faces of the wing. There is no inlet flow, and an outlet boundary condition is applied to the entire outer boundary of the fluid domain. The mesh partition of the fluid domain is shown in Fig. 17. The numbers of linear tetrahedral elements and nodes are 404,159 and 273,392, respectively. The radius of the fluid domain is set to be 20 times larger than the length of the wing. We also design the fluid mesh such that the mesh size decreases from the outer boundary to the inner boundary and the stiffness increases as the mesh size decreases, effectively reducing the distortion of smaller elements near the wing. Because of this mesh control technique, most of the distortion of the mesh caused by the flapping motion of the wing occurs in larger elements far from the wing, where as smaller elements near the wing are not significantly distorted. This requires a larger fluid analysis domain but stabilizes the FSI analysis without remeshing the fluid domain. The mesh partition of the structure domain is shown in Fig. 18. Here the numbers of quadratic tetrahedral elements and nodes are 154,080 and 243,243, respectively.

The properties of the analysis model are as follows. The dynamic viscosity and density of the fluid are 0.0544 and 1.0, respectively. The Young's modulus of the elastic part of the wing is a design variable, ranging from 0 to 10^{-4}, and that of the rigid part is 10^{-4}. The density of the structure is 5.34 x 10^{-10}. The parameters used in the simulation are given as dimensionless parameters because the flow solver FFB treats parameters as dimensionless quantities. However, we can give units to the parameters and values of the analysis results for a particular purpose after the analysis. A PC cluster is used for this analysis. It consists of four PCs, each of which has a 3.4 GHz quad-core Intel i7 2600 processor and 16 GB of DDR3 memory. The initial velocity and pressure in the fluid domain were both set to 0. We perform four iterations of the FSI analysis with different design variables, i.e. the Young's modulus of the elastic part of the wing (1.7 x 10^{-6} and 2.5 x 10^{-6}) and the maximum angle of flapping (30^o and 45^o). In all cases, the flapping frequency and time step were set to 0.8 and 1.25 x 10^{-3}sec, respectively. The convergence criterion $\varepsilon_{tol} = 10^{-3}$ was used in the fixed point iteration. An average of three iterations were required for each time step. The fluid force on the wing surface at each time step and the time averaged fluid force on each axis are calculated as :

$$\boldsymbol{F}_t = (F_t^x, F_t^y, F_t^z) \tag{13}$$

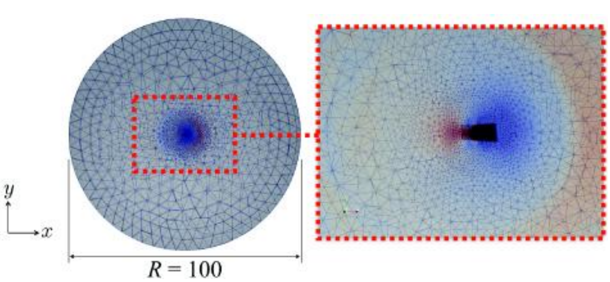

Fig. 17: Mesh partition of the fluid domain

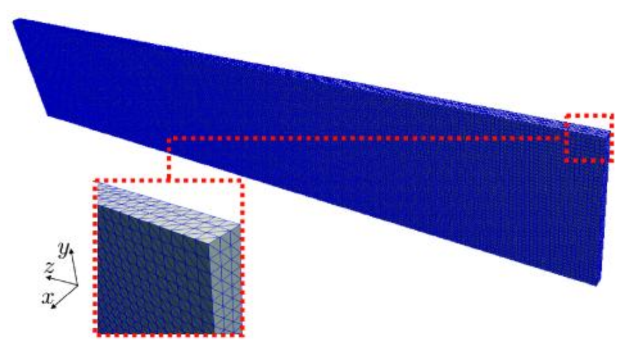

Fig. 18: Mesh partition of the structure domain

$$F_{avg}^{i} = \frac{\sum_{t=t'}^{t'+(n-1)\Delta t} F_t^i}{n} \left(n = \frac{T}{\Delta t} \right) \qquad (14)$$

where $\boldsymbol{F}_t$ is the fluid force vector on the wing surface at time t, F_t^i is the fluid force at time t on each axis ($i = x,y,z$), F_{avg}^i is the time-averaged fluid force on each axis, t' is the standard time step for evaluation, Δt is the time step, and T is the flapping period. The time-averaged fluid force vector is defined as :

$$F_{avg} = \left(F_{avg}^{x}, F_{avg}^{y}, F_{avg}^{z} \right) \qquad (15)$$

We applied a lift force along the vertical direction, which maximizes the force and is defined as :

$$\alpha = \arctan\left(\frac{F_{avg}^{y}}{F_{avg}^{x}} \right) \qquad (16)$$

$$F_{lift} = F_x \sin\alpha + F_y \cos\alpha \qquad (17)$$

$$F_{drag} = F_x \cos\alpha + F_y \sin\alpha \qquad (18)$$

where α is an angle with respect to the y-axis in the xy plane that defines the vertical direction, F_{lift} is the lift force, and F_{drag} is the drag force.Various values, including the lift and drag forces, were calculated to evaluate the flight performance. The visualized results, shown in Fig. 19, helped us to understand the mechanism that enhances the lift and reduces the drag.

Figure 19 shows that leading edge vortices that developed and contributed to increase the lift when the translational velocity of the wing was high. The lines and blue contours indicate streamlines and low-pressure (threshold: –30) areas, respectively.

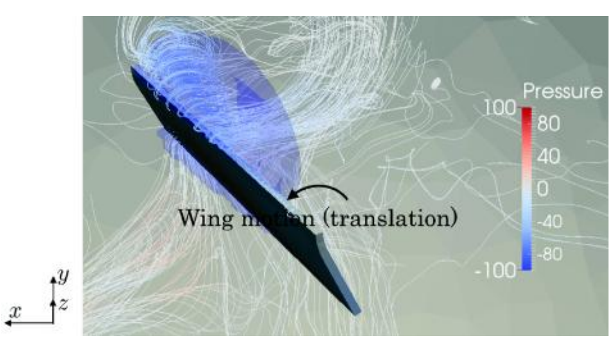

Fig. 19: Snapshot of pressure and streamlines. Contour color shows pressure (Blue-negative). The maximum angle of flapping is 30°, and the coefficient of the Young's modulus of E is 0.0075

Figure 20 shows the definition of the passive feathering angle between two lines of the elastic part of the wing and a line normal to the leading edge. The passive feathering angle indicates the degree of deformation of the wing. Because the elastic part of the wing has a low Young's modulus (1.7 x 10^{-6}), it deformed more than that with high Young's modulus (2.5 x 10^{-6}), as shown in Fig. 21. The lift increased when the maximum flapping angle changed from 30° % to 45° %, as shown in Fig. 22, because a phase difference developed between the flapping and passive feathering angles depending on the maximum flapping angle in Fig. 21. However, significant deformation does not always enhance the lift force. Using the developed FSI analysis system, we will be able to accumulate knowledge on the quantitative relations between various design parameters and the flight performance of a flapping wing.

Flow-Induced Vibration and Noise of Automobile

Reduction of interior noise is an important issue for driver's comfort of a car. Interior noise can be reduced

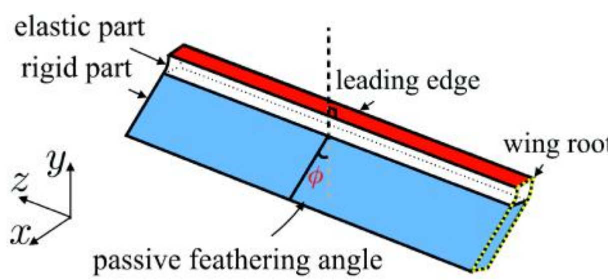

Fig. 20: Definition of the passive feathering angle

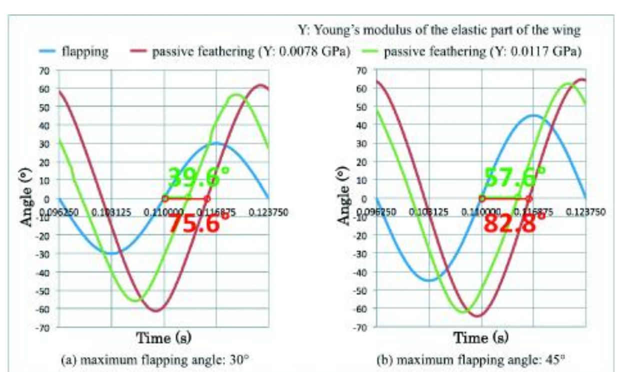

Fig. 21: Time histories of the flapping and passive feathering angles

by absorption and/or insulation of the transmitted sound. However, these methods are most likely to result in increasing in a production cost. It is generally required to reduce the interior noise under the limited design conditions, and for doing so, it is important to predict interior noise and to understand dominant sources and propagation paths of the interior noise. Interior noise of a car can be classified into engine noise, road noise, and aeroacoustical noise.

To predict aeroacoustical interior noise of a car by numerical simulations, we need to predict pressure fluctuations on the external surfaces of a car, which is the main source of the noise, at the first step. We then need to compute propagation of sound by vibration in the car body, and finally acoustical field in the cabin. Statistical Energy Analysis (SEA) has been widely applied to evaluate propagation of sound through the car body and the acoustical field (for example, Kosaka *et al.*, 2013; Chen *et al.*, 2011). In SEA, the computational domain is decomposed into several subdomains and the vibration and interior noise are computed by assuming the equilibrium power balance among the input, dissipated and transmitted power for each subdomain. The computational model for SEA includes equivalent mass, inner dissipation coefficient, and coupling dissipation coefficient. These coefficients are determined by analytical, numerical and/or experimental method.

In our study (Yamade *et al.*, 2016; Iida *et al.*, 2016), we performed one-way coupled simulation instead of SEA. We computed directly vibration in the car body and sound fields in the cabin to investigate and understand the propagation paths of vibration and sound.

At first, car body surface pressure was predicted as input force of vibrational analysis. The flow solver used is an incompressible flow solver, FFB (Kato *et al.*, 2003, 2005). The pressure fluctuations computed here do not include acoustic pressure fluctuations. Schell and Cotoni reported in Ref. (Schell and Cotoni, 2015) that external acoustic pressure fluctuations become main contributor of the interior noise in a high frequency range around 1 kHz. Therefore the present method might underpredict interior noise at the high frequency range.

Next the structural vibration analysis and the acoustical analysis were performed, together with the comparison with wind tunnel experimental results. The structure solver is a commercial version of ADVENTURE, i.e. ADVENTURECluster (Akiba *et al.*, 2006).

The final step is the prediction of the acoustical field in the cabin. The vibration accelerations on the internal surfaces of the test car computed by the structural analysis were fed to the acoustical analysis.

FFB-ACOUSTICS (FFB-A)(Guo *et al.*, 2015), which is an in-house FEM-based acoustical solver, was used to perform the acoustical analysis in the frequency domain. The solver was primarily designed to solve Lighthill's equation (Lighthill, 1952) that represents sound propagation. The acoustical solver can deal with not only quadrupole sources of sound distributed in a computational domain but also vibration accelerations distributed on a boundary of a computational domain. Note in this study, quadrupole sources of sound in the cabin were not considered. Instead, vibration accelerations computed by the structural analysis were fed as boundary conditions for predicting a sound field in the cabin.

In the present one-way coupling analysis, the REVOCAP_Coupler (Yoshimura *et al.*, 2008), which is a family of ADVENTURE_Coupler, was employed. Time dependent pressure fluctuations on the exterior surfaces of the vehicle are calculated by the flow solver, which simulates turbulent flow of air around the vehicle. These surface pressure fluctuation data on the mesh surfaces of the CFD analysis are mapped onto the mesh surfaces of the structural analysis. Appropriate mesh sizes for the flow solver are different from those for the structural solver. In our research, a kei-car in which interior and under-floor were simplified was employed to the wind tunnel tests as well as for the computational analyses. The wind tunnel tests were performed with the main stream velocity of 100km/h (Yamade *et al.*, 2016; Iida *et al.*, 2016).

Numerical Results

By the flow solver, pressure fluctuations on the exterior surfaces of the test car were calculated for two mesh models. That is, mesh model A, composed of 80 million grids and mesh model B, composed of 5 billion grids. The results of mesh model A is named as "fluid model A", while that of the mesh model B as "fluid model B". The total number of DOFs of the structural analysis mesh is about 14.7 millions. The mesh is mainly composed of triangular shell elements with some other types of elements such as solid elements and beam elements. The computational conditions of the vibration structure analysis are given in Table 1. The magnitude of response acceleration as a function of frequency is compared with the measured value in Fig. 22(A)-(C) at the sampling points in the windshield, the backdoor glass, and the backdoor panel along the center line. The green lines indicate the measured values, and the red ones show the results obtained by using fluid model B, and the indigo blue ones those by fluid model A. The predicted values have been averaged by 5 times with 75 % overlap using a total step of 4,096. The frequency resolution in the experiment is about 4 Hz, and that of the analyses is about 4.5 Hz. As can be seen from the figure, both results agree reasonably well with each other on the broad peak around at 30 Hz on the backdoor glass and the backdoor panel. In Fig. 22(D)-(G), the magnitude of response acceleration is compared with the measured value as a function of frequency. The sampling points are set in the glass of the front and rear side doors and in those of side door panels.

In the acoustical analysis model, the minimum mesh size is 1mm, the maximum mesh size is 4 mm, and the PPW (points per wave) is 20 at 4 kHz. This mesh model can resolve an acoustic wave up to 4 kHz. The number of the finite elements is 38 millions. The vibration velocities that were computed by the structural analysis were decomposed into 512 frequency bands ($\Delta f = 9$ Hz) because the acoustical analysis was performed in the frequency domain. As already mentioned, all the interior components, such as seats, carpet, and plastic trims were removed, and therefore hard-wall boundary conditions were prescribed there. No spatial damping effects on the sound waves are considered in the present acoustical analysis. The calculated sound pressure level was averaged 7 times for each frequency. The computational conditions of the acoustical analysis are shown in Table 2.

Figure 23 shows contour maps of interior acoustic pressure and exterior velocity magnitude in the plane of symmetry of the test car. At low frequency bands up to 315 Hz, longitudinal and vertical predominate modes were observed in the cabin. At

Table 1: Computational conditions and resources needed for present structual vibration analysis

Computational grid	Number of elements	2.5×10^6
	Number of DOFs	14.7×10^6
	Min.grid resolution[mm]	5.0
CPU used	Model	Hitachi CX1000
	Number of Cores	96
Time integration	Time Increment [sec]	108.0
	Total time steps computed [-]	4,100
	Time Increment computed total time steps [sec]	0.4428
Computation time	Computation time per step [sec]	46.7
	Total computation time [hours]	53

Table 2: Computational conditions and resources needed for present acoustical analysis

Computational grid	Number of grids	38×10^6
	Grid resolution [mm]	4.0
CPU used	Model	Fujitsu FX10
	Number of Cores	1536
FFT	Lines	512
	Upper frequency [Hz]	5000
	Lower frequency [Hz]	100
Computation time	Total computation time [hours]	21

frequency bands over 630 Hz up to 1 kHz, for which the wave length of the sound is relatively short, no predominate mode was observed in the cabin. Local peaks with high and low values were distributed randomly at high frequency bands over 1 kHz. It is difficult to identify the region from where the noise is intruded from outside only by these maps of sound pressure distributions.

Conclusions

Leading supercomputers offer the computing power of petascale, and exascale systems are expected to appear in the end of this decade. Supercomputers with more than tens of thousands of computing nodes, each of which has many cores, cause serious problems in practical finite element software. Not only the time consuming hot spots of the algorithms

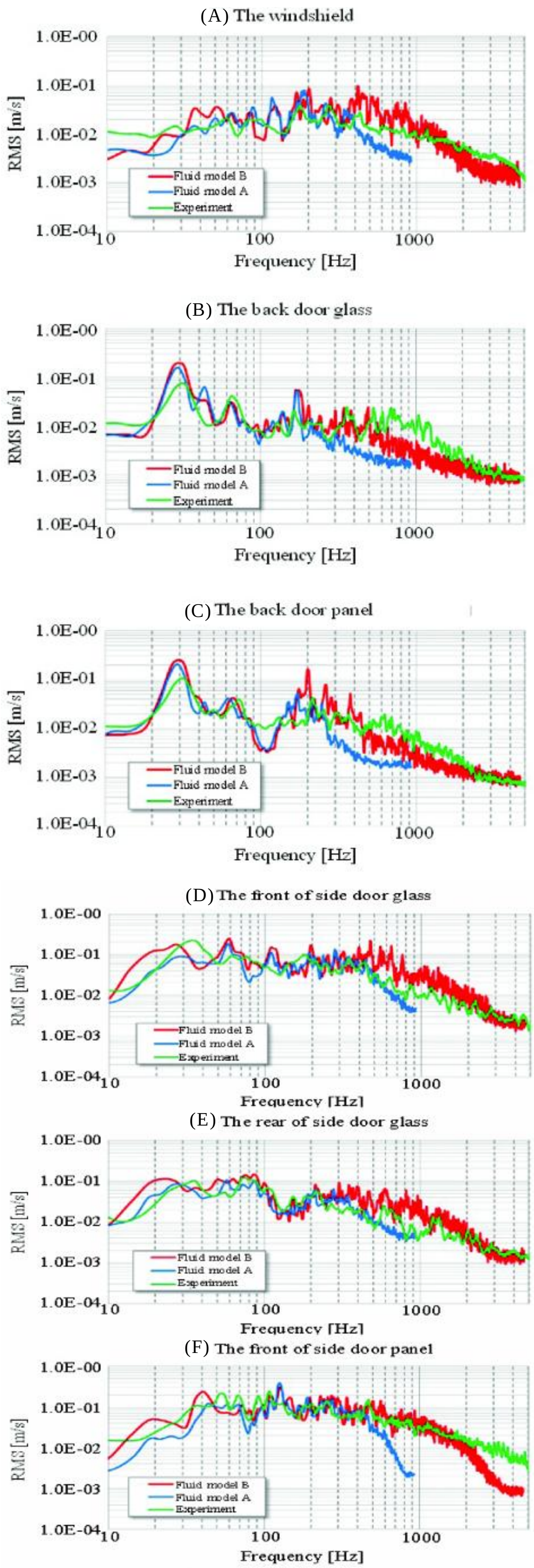

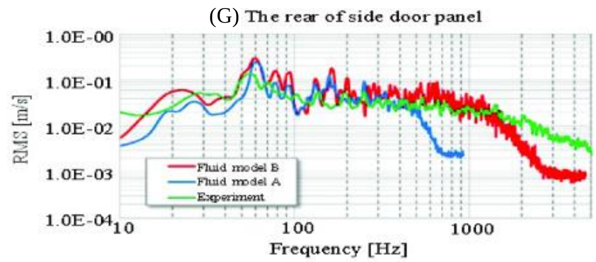

Fig. 22: Comparison between predicted and measured response accelerations. (A) wind shield, (B) backdoor glass and (C) backdoor panel, (D) front side-door glass, (E) rear side-door glass (F) front side-door panel and (G) rear side-door panel

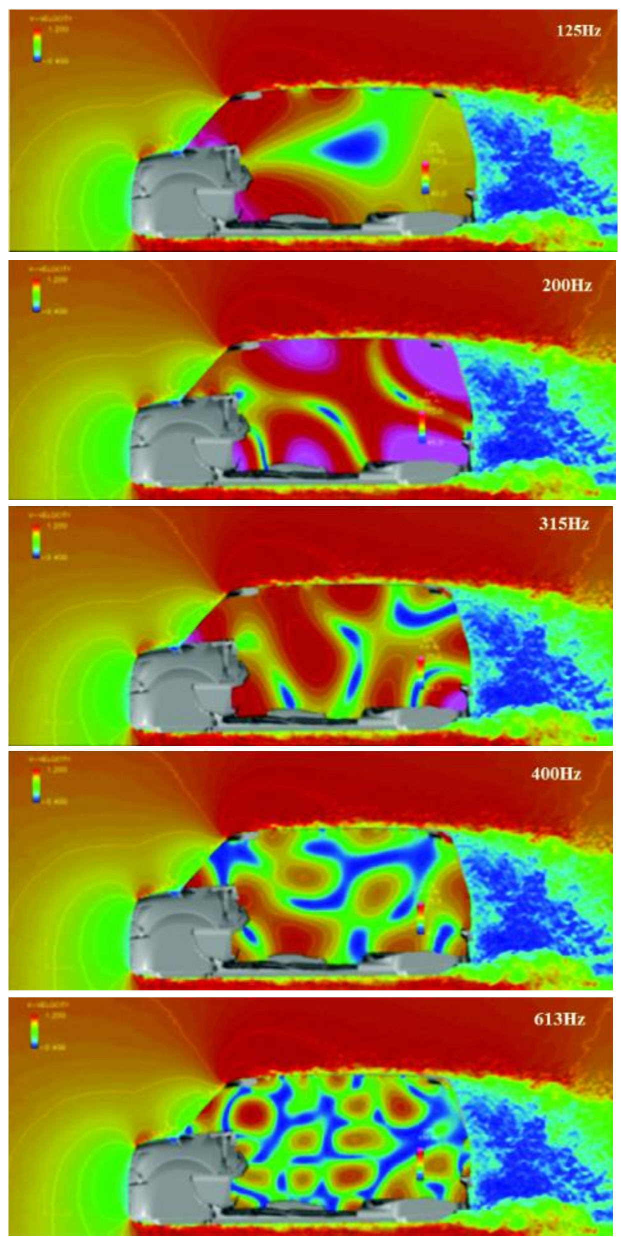

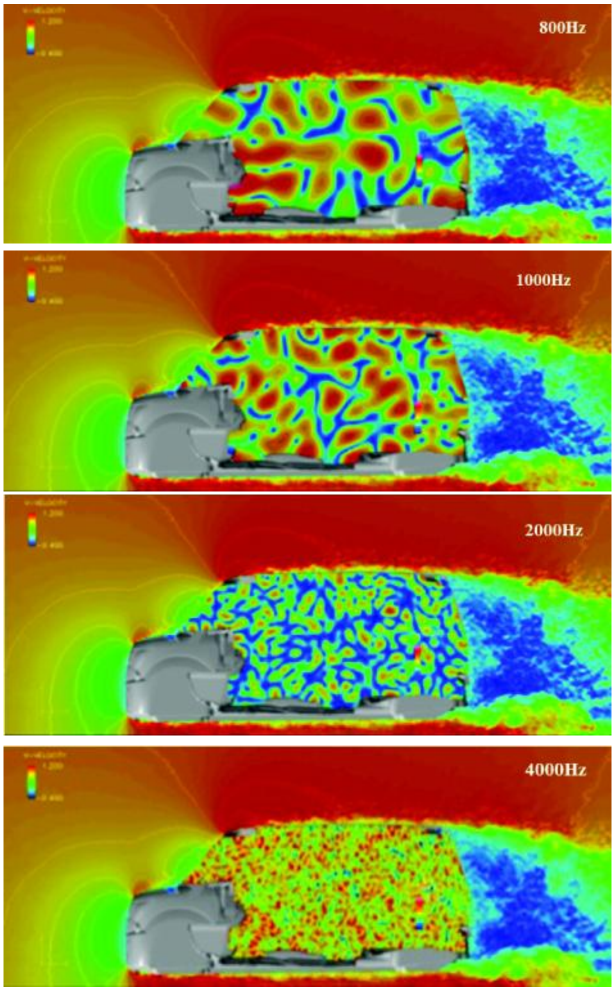

Fig. 23. Contours of sound pressure level in the cabin and exterior velocity magnitude at plane of symmetry

but also the entire algorithms must be well tuned and parallerized. For example, K computer, a Japanese Petaflops machine consists of 88,128 processing nodes and 705,024 cores, and achieves peak performance of 10.5 Peta FLOPS. Latest HPC machines require the following three-layered parallelisms, i.e. (1) Speedup within core, (2) Parallelism in inter-node : Increase parallel efficiency in multicore calcuation considering memory band width, and (3) Parallelism in intra-node: Increase parallel efficiency in intra-node calculation considering intra-node communication speed.

Furthermore, we have been developing a general-purpose platform of parallel partitioned coupling techniques with nonlinear iteration, which ensure accuracy, high parallel-efficiency, robustness as well as flexibility. The ADVENTURE's parallel solvers together with the coupling platform enable large-scale parallel coupled analyses of very complicated structures including Fluid-Structure Interaction, Acoustic Fluid-Structure Interaction, Magneto-Structure Interaction and Structure-Structure Interaction. The technologies developed here would become de Fact Standard of large scale coupled finite element analyses for high-performance computing of peta to exaflops scale.

References

Akiba H, Yoshimura S *et al*. (2006) Large scale drop impact analysis of mobile phone using ADVC on Blue Gene/L *Proceedings of IEEE/ACM Supercomputing'06,* CD-ROM

Bazilevs Y, Takizawa K and Tezduyar T E (2013) Computational Fluid Structure Interaction : Methods and Applications Wiley

Charles G and Broyden A (1965) A class of methods for solving nonlinear simultaneous equations *Mathematics of Computation* **19** 577-593

Chen S M, Wang D F and Zan J M (2011) Interior noise prediction of the automobile based on hybrid FE-SEA method *Mathematical Problems in Engineering* **1** 1-20

Degroote J, Bathe K J and Vierendeels J (2009) Performance of a new partitioned procedure versus a monolithic procedure in fluid-structure interaction *Computers & Structures* **87** 793-801

Dettmer W and Peric D (2006) A computational framework for fluid-structure interaction: finite element formulation and applications *Computer Methods in Applied Mechanics and Engineering* **195** 5754-5779

Felippa C A and Park K C (1980) Staggered transient analysis procedures for coupled mechanical systems: Formulation *Computer Methods in Applied Mechanics and Engineering* **24** 61-111

Forster C, Wall W and Aramm E 2007 Artificial added mass instabilities in sequential staggered coupling of nonlinear structures and incompressible viscous flows *Computer Methods in Applied Mechanics and Engineering* **196** 1278-1293

Guo Y, Kato C, Yamade Y and Ohta Y (2015) Computation of noise from internal flow in a centrifugal blower *Proceedings of The 13th Asian International Conference on Fluid*

Machinery AICFM13-137

Heil M (2004) An efficient solver for the fully-coupled solution of large-displacement fluid-structure interaction problems *Computer Methods in Applied Mechanics and Engineering* **193** 1-23

Iida K, Onda K, Iida A, Kato C and Yoshimura S (2016) Prediction of aeroacoustical interior noise of a car, part-2structural and acoustical analyses *SAE Technical Paper* 2015-01-0235

Ishihara D and Yoshimura S 2005 A monolithic approach for interaction of incompressible viscous fluid and an elastic body based on fluid pressure Poisson equation *International Journal for Numerical Methods in Engineering* **64** 167-203

Jiang Y Y, Yoshimura S, Imai R, Katsura H, Yoshida T and Kato C (2007) Quantitative evaluation of flow-induced structural vibration and noise in turbomachinery by full-scale weakly coupled simulation *Journal of Fluids and Structures* **23** 531-544

Kataoka S, Minami S, Kawai H, Yamada T and Yoshimura S (2014) A parallel iterative partitioned coupling analysis system for large-scale acoustic fluid-structure interactions *Computational Mechanics* **53** 1299-1310

Kato C, Kaiho M and Manabe A (2003) An overset finite-large-eddy-simulation method with application to turbomachinery and aeroacoustics *Trans ASME Journal of Applied Mechanics* **70** 32-43

Kato C, Yamade Y, Wang H, Guo Y, Miyazawa M, Takaishi T and Yoshimura S (2005) Numerical prediction of sound generated from flows with a low Mach Number *Computers and Fluids* **36** 53-68

Kosaka F, Okutsu Y, Hamamoto N and Shiozaki H (2013) An SEA modeling for wind using wavenumber-frequency spectrum *Transactions of Japan Society of Mechanical Engineers* **79C** 3691-3709

Küttler U and Wall W A (2008) A fixed-point fluid-structure interaction solvers with dynamic relaxation *Computational Mechanics* **43** 61-72

Küttler U and Wall W A (2009) Vector extrapolation for strong coupling fluid structure interaction solvers *Journal of Applied Mechanics* **76** 1-7

Le Tallec P and Mouro J 2001 Fluid structure interaction with large structural displacements *Computer Methods in Applied Mechanics and Engineering* **190** 3039-3067

Lighthill M J (1952) On sound generated aerodynamically. I General theory *Proc R Soc London A* **211** 564-587

Mandel J (2002) An iterative substructuring method for coupled fluid-solid acoustic problems *Journal of Computational Physics* **177** 95-555

Matthies H G, Niekamp R and Steindorf J 2006 Algorithms for strong coupling procedures *Computer Methods in Applied Mechanics and Engineering* **195** 2028-2049

Michler C, van Brummelen E H and de Borst R (2004) An interface Newton Krylov solver for fluid-structure interaction *International Journal for Numerical Methods in Fluids* **47** 1189-1195

Minami S and Yoshimura S (2010) Performance evaluation of nonlinear algorithms with line search for partitioned coupling technique for fluid structure interactions *International Journal for Numerical Methods in Fluids* **64** 1129-1147

Minami S, Kawai H and Yoshimura S (2011) A monolithic approach based on the balancing domain decomposition method for acoustic fluid-structure interaction *Journal of Applied Mechanics* **79** 010906

Mittal S and Tezduyar T E (1992) A finite element study of incompressible flows past oscillating cylinders and aerofoils *International Journal for Numerical Methods in Fluids* **15** 1073-1118

Nakata T and Liu H (2012) A fluid-structure interaction model of insect flight with flexible wings *Journal of Computational Physics* **231** 1822-1847

Nuclear Power Engineering Center (NUPEC) 1988 Seismic proving test of the reactor internals of BWR *Report of Proving Tests on the Reliability for Nuclear Power Plant*

Ogino M, Shioya R, Kawai H and Yoshimura S (2005) Seismic response analysis of full scale nuclear vessel model with ADVENTURE system on the Earth Simulator *Journal of the Earth Simulator* **2** 41-54

Ohayon R (2001) Reduced symmetric models for modal analysis of internal structural-acoustic and hydroelastic-sloshing systems *Computer Methods in Applied Mechanics and Engineering* **190** 3009-3019

Park K C, Felippa C and AOhayon R (2001) Partitioned formulation of internal fluid-structure interaction problems by localized Lagrange multipliers *Computer Methods in Applied Mechanics and Engineering* **190** 2989-3007

Schell A and Cotoni V (2015) Prediction of noise in a sedan due to exterior flow *SEA International Journal Passenger Cars-Mechanical Systems* **8** doi:4271/2015-01-2331

Takizawa K, Tezduyar T E and Kostov N 2014 Sequentially-coupled space-time FSI analysis of bio-inspired flapping-wing aerodynamics of an MAV *Computational Mechanics* **54** 213-233

Takizawa K, Tezduyar T E and Buscher A (2015) Space-time computational analysis of MAV flapping-wing aerodynamics with wing clapping *Computational Mechanics* **55** 1131-1141

Tezduyar T E, Sathe S, Keedy R and Stein K (2006) Space-time finite element techniques for computation of fluid-structure interactions *Computer Methods in Applied Mechanics and Engineering* **195** 2002-2027

Yamada T and Yoshimura S (2008) Line search partitioned approach for fluid structure interaction analysis of flapping wing *Computer Modelling in Engineering & Sciences* **24** 51-60

Yamada T, Hong G W, Yoshimura S and Kataoka S Parallel partitioned coupling analysis system for large-scale incompressible viscous fluid-structure interaction problems *Computers and Fluids* Accepted for Publication

Yamade Y, Kato C, Yoshimura S, Iida A, Iida K, Onda K, Hashizume Y and Guo Y (2016) Prediction of aeroacoustical interior noise of a car, part-1 prediction of pressure fluctuations on external surfaces of a car *SAE Technical Paper* 2015-01-0401

Yoshimura S, Shioya R, Noguchi H and Miyamura T (2002) Advanced general-purpose computational mechanics system for large-scale analysis and design *Journal of Computational and Applied Mathematics* **49** 279-296

Yoshimura S, Yamada T and Yonemura N (2008) REVOCAP_Coupler : General purpose CAE platform for large scale coupled analyses *Proceedings of Japan Society of Mechanical Engineerings* **11** 902-903

Yoshimura S, Yamada T, Kawai H, Miyamura T, Ogino M and Shioya R (2015a) Petascale Coupled Simulations of Real World's Complex Structures *IACM Expression* **37** 9-13

Yoshimura S, Hori M and Ohsaki M (2015b) *High-performance computing for structural mechanics and earthquake/ Tsunami Engineering* Springer

Yoshimura S, Yamada T, Koide Y, Onitsuka S and Iijima T (2015c) Full scale simulation-based study on dynamic response of BWR fuel assemblies under seismic loading, Proceedings of ASME 2015 PVP Division Conference, Boston, PVP2015-45334

Zhang Q and Hisada T (2001) Numerical methods for FSI problems with strong dependence between fluid and structure *Computer Methods in Applied Mechanics and Engineering* **190** 6341-6357.